

Spatial maps in piriform cortex during olfactory navigation

<https://doi.org/10.1038/s41586-021-04242-3>

Cindy Poo¹✉, Gautam Agarwal², Niccolò Bonacchi¹ & Zachary F. Mainen¹✉

Received: 16 October 2020

Accepted: 12 November 2021

Published online: 22 December 2021

 Check for updates

Odours are a fundamental part of the sensory environment used by animals to guide behaviours such as foraging and navigation^{1,2}. Primary olfactory (piriform) cortex is thought to be the main cortical region for encoding odour identity^{3–8}. Here, using neural ensemble recordings in freely moving rats performing an odour-cued spatial choice task, we show that posterior piriform cortex neurons carry a robust spatial representation of the environment. Piriform spatial representations have features of a learned cognitive map, being most prominent near odour ports, stable across behavioural contexts and independent of olfactory drive or reward availability. The accuracy of spatial information carried by individual piriform neurons was predicted by the strength of their functional coupling to the hippocampal theta rhythm. Ensembles of piriform neurons concurrently represented odour identity as well as spatial locations of animals, forming an odour–place map. Our results reveal a function for piriform cortex in spatial cognition and suggest that it is well-suited to form odour–place associations and guide olfactory-cued spatial navigation.

Olfaction is critical for animals navigating their environments in search of valuable resources¹. Animals instinctively use odour memories to guide spatial choices⁹ and odours are widely used in the study of spatial memory and navigation¹⁰. Cortical structures for odour perception and spatial memory are evolutionarily and developmentally linked, together forming the allocortex (consisting of olfactory, hippocampal and entorhinal cortices). Olfaction and spatial memory systems are therefore intimately related, as reflected by animal behaviour, evolution and circuit anatomy. Moreover, while the primary olfactory (piriform) cortex receives direct sensory input via olfactory bulb projection neurons, its three-layered circuit architecture shares striking resemblances to the hippocampus, with broadly distributed and unstructured recurrent connections that are highly plastic^{11–16}. This has prompted conjectures that these structures implement similar learning functions^{11,17–19}. Given its circuit architecture and connectivity, if spatial information were present in the piriform cortex (PCx) it would be well-positioned to function as part of the spatial memory system.

PCx is divided into anterior PCx (aPCx) and posterior PCx (pPCx) regions^{20,21}. While both regions are characterized by recurrent circuitry, aPCx receives more inputs from the olfactory bulb and other olfactory regions and is thought to underlie odour identification and discrimination^{3,4,22–24}, whereas pPCx is more strongly connected to higher-order associative regions and much less is known about its function^{13,21,25–29}.

Odour-cued spatial choice task

We developed an odour-cued spatial choice task that challenged rats to use spatial information along with odour identity to navigate to a specific location for reward. We made recordings from pPCx and area CA1 of the hippocampus in rats performing this task (Fig. 1 and Extended Data Fig. 1). Our behavioural arena consisted of an elevated

plus-maze with a 1 m² footprint positioned in a room with visual landmarks. At the end of each arm was a port that could deliver either an odour cue or a water reward. Trials began when an LED was activated at one of the four ports. Rats learned to insert their snouts into the lighted port in order to receive randomly one of four odours (Fig. 1a, b and Supplementary Video). Odours were transiently available when the rats held their snout within the sampling port (Fig. 1b). The rats then had to navigate to the spatial goal associated with that odour to collect water reward (Fig. 1c and Extended Data Fig. 2). Critically, trial initiation cues were randomly interleaved across all four ports, encouraging rats to adopt a location-based (allocentric) strategy over a direction-based (egocentric) action rule (Fig. 1e). Performance was similar across odours, choice locations and choice directions after training (Fig. 1d).

This task differs from most sensory-cued decision tasks, which use spatial responses (for example, left versus right choice) that do not require use of a spatial map because they can be solved by directly associating an odour cue with an action. A signature of such tasks is that animals show a win-stay bias, repeating a successful action following reward³⁰. Here, rats instead showed a bias to return to the same location following a successful trial, but no bias to repeat the same action (Fig. 1f, g, 6 rats, approximately 40,000 trials; Methods). This suggests that rats use allocentric spatial maps in conjunction with olfaction in this task. Notably, the rats performed with higher accuracy when the odour-cued goal location was congruent with odour sampling location (Extended Data Fig. 2c, d).

Odour locations are encoded in piriform cortex

We recorded from pPCx using chronically implanted tetrodes, and found that neurons fired differently depending on both odour identity

¹Champalimaud Foundation, Lisbon, Portugal. ²W. M. Keck Science Center, The Claremont Colleges, Claremont, CA, USA. ✉e-mail: cindy.poo@neuro.fchampalimaud.org; zmainen@neuro.fchampalimaud.org

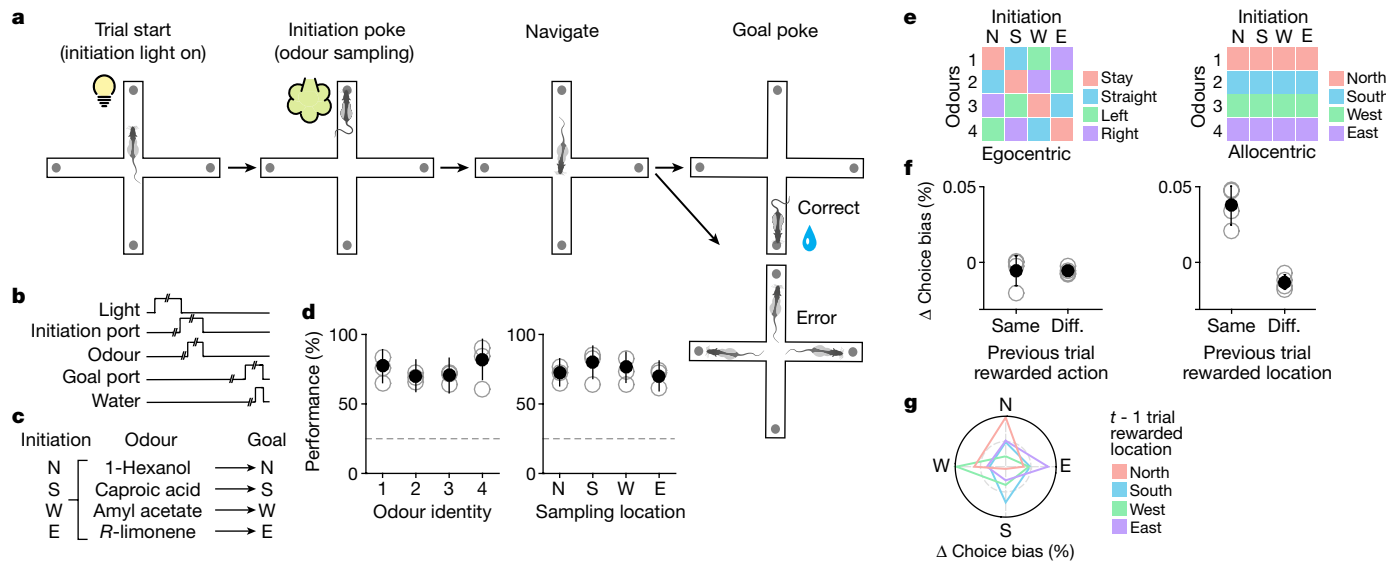


Fig. 1 | Odour-cued allocentric spatial choice task. **a**, Schematic of trial structure. **b**, Temporal events in trials. **c**, Relationships of odour to reward location. Each odour can be sampled at any initiation port. Odour identity determined the location at which water reward was available. **d**, Behavioural performance of rats was similar across all odours and initiation (odour-sampling) locations. Chance performance was 25% (grey dashed lines). **e**, Schematic illustrating the egocentric (left) or allocentric (right) rules that rats must follow in order to correctly perform the task given all possible odour and sampling

locations. **f**, Left, reward for a particular action does not bias the choice probability for the same action in the following trial. Right, reward at a particular location biases the choice probability towards the same location in the following trial. Diff., different. **g**, Given a reward at specific port locations, rats were positively biased towards choosing the same location on subsequent trials (Methods). The dashed grey circle on the polar plot marks 0 (the level of chance), and the black circle marks 0.05 above chance.

and the location of sampling (Fig. 2a–d). Individual neurons displayed a range of selectivity, from strictly spatial (Fig. 2a) to purely odour selective (Fig. 2b). Across the entire set of recordings, we found that more pPCx neurons were selective for port location than for odour identity (40% versus 29%; Fig. 2e). Selectivity properties did not correlate with extracellular electrophysiological signatures associated with cell types such as spike waveform or overall firing rate. To test for the possibility that the spatially restricted firing of pPCx neurons reflected stray odours on the maze³¹ (potentially deposited by the rat), each recording session was split into two blocks, separated by a 15–20 min interval during which maze and ports were thoroughly cleaned with disinfectant and an enzymatic cleaner (Methods). Spatial firing rates of individual neurons across the two blocks within a session were stable across locations (Extended Data Fig. 3).

Overall, mean firing rates of pPCx neurons were low³² (Extended Data Fig. 4a, top). There were no differences in firing rates between the subpopulations of neurons that had odour, location or joint selectivity (Extended Data Fig. 4a, b). The sparseness of odour responses, which is a measurement of response selectivity, was somewhat lower (less sparse) than those reported previously in aPCx^{3,22} (Extended Data Fig. 4e). We did not see systematic biases in behaviour or neural responses that might result from non-uniform availability of odours (Fig. 1d and Extended Data Fig. 4b–d). Correlation analysis of population response vectors showed that the pPCx population encodes spatial locations more distinctly than odours (Fig. 2f and Extended Data Fig. 5a, b). There was no systematic relationship between how odours and locations were represented across the population. For example, population response vectors were not more similar between odour 1 and the north port (Extended Data Fig. 5a).

We quantified the spatial representations by using linear classifiers to understand how well a downstream observer could decode odour identity or spatial location of the animal by observing firing rates of pPCx neurons (Methods). Pooling all recorded neurons across sessions, both odour identity (Fig. 2g, left, black line) and odour sampling locations could be successfully decoded (Fig. 2g, right, black line). Similar

results for odour decoding were obtained when pPCx spike times were aligned to first inhalation after odour onset (Extended Data Fig. 6a). Linear classifiers trained using only simultaneously recorded neurons were able to decode odour identity and spatial locations across time, showing that both odours and spatial locations are concurrently represented in piriform (Fig. 2h).

These results indicate that pPCx neurons are involved in representing both spatial location and odour identity and that many more pPCx neurons are required to reach a given level of odour-decoding accuracy compared to what has been observed for aPCx using similar methods^{3,22–24}. At the level of individual neurons, port locations were on average better encoded than odour identities (Extended Data Fig. 5d). Therefore, at least in the context of our task, odour coding in pPCx could be considered fairly poor, consistent with a previous report³². In this method of pseudo-population decoding, the decoder randomly samples neurons in the population. If instead one uses a decoder which selects the most informative neurons first using sparse regularization, or if the decoder used responsive neurons first identified from ROC analysis, then fewer numbers of neurons were required to reach a decoding accuracy of around 90% for both odours and locations (Fig. 2g, grey lines, and Extended Data Fig. 6c–f; Methods). Therefore, our results are consistent with the possibility that a downstream area listening to the right subset of pPCx neurons could effectively extract odour information.

Piriform spatial selectivity is stable and robust

The time course of location-decoding accuracy in pPCx began well ahead of odour delivery, suggesting that spatial coding in pPCx does not depend on olfactory drive (Fig. 2h and Extended Data Fig. 7). However, the prominence of spatial selectivity around the odour ports also suggests the possibility that it might reflect task-related odour-predictive signals²⁷. In this case, we would expect them to be specific to this epoch of the task. Alternatively, spatial information could be represented akin to a cognitive map of space^{33,34}, in which case, we would expect to see

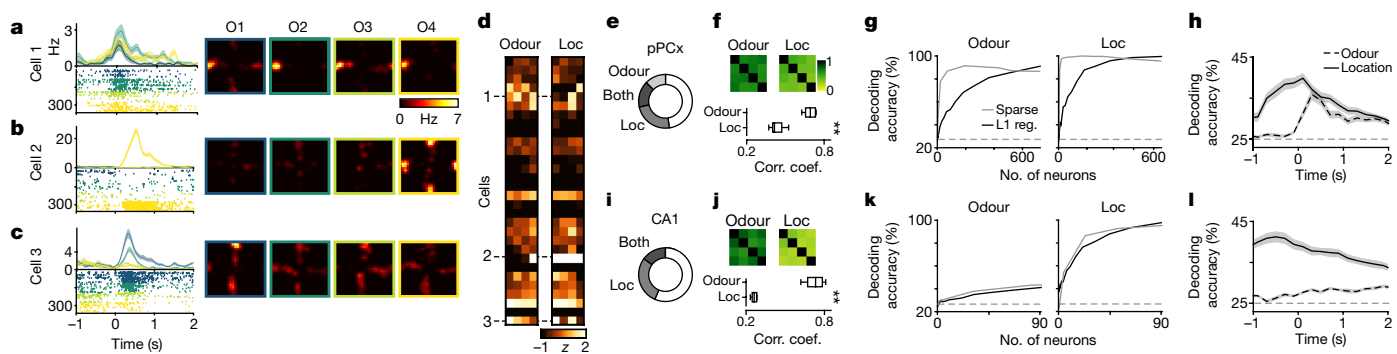


Fig. 2 | Spatial representations in the piriform cortex. **a–c**, Left, peri-event time histogram and raster plots aligned to odour onset for three example neurons recorded in one session for four odours. Right, firing-rate heat maps normalized for occupancy were generated by concatenating all trials for an individual odour from -1 to 2 s around initiation port entry (Methods). **d**, Z-scored firing rates of simultaneously recorded pPCx population in example session ($n=30$ cells). Loc, location. **e**, Selectivity of piriform neurons for odours, locations, or both. **f**, Top, population correlation similarity matrix obtained by computing the pairwise Pearson's correlation coefficients for population response vectors across four odours (left) and port locations (right). Squares along the diagonal band represent autocorrelation. **f**, Bottom,

population correlation coefficients (corr. coef.) excluding autocorrelation coefficients of the diagonal band, for odours, 0.69 ± 0.04 ; for locations, 0.43 ± 0.05 (Wilcoxon rank-sum test, $P < 0.001$). Box plots show median, 25th and 75th percentiles, and whiskers indicate the range of data points. **g**, Decoding accuracy of linear classifiers for odour identity and location. For further discussion, see Extended Data Fig. 6c, d. **h**, Decoding accuracy across time for location and odour identity for simultaneously recorded populations (mean \pm s.e.m., $n=33$ sessions; 30 ± 13 neurons per session). **i–l**, Similar analysis as in **e–h** for CA1 (154 cells, 15 sessions, 8 ± 1 cells per session).

representation of a spatial environment that is consistent across task epochs. To examine this, we compared the spatial selectivity of neurons around the two different kinds of task-related nose poke events, the initiation of the trial (when an odour is anticipated), and the arrival at goal (when a reward is anticipated). Consistent with the ‘cognitive map’ hypothesis, spatial properties of individual neurons remained constant across these two different task epochs (Fig. 3a–c). Similarity matrices for population response vectors demonstrated the stability of pPCx location representation, as reflected by the diagonal axis of higher correlation coefficients (Fig. 3b). Indeed, a linear classifier trained using population activity during the initiation epoch was able to successfully decode location from neural activity during the reward epoch (Fig. 3c). This result held true even for neural activity during the inter-trial interval (Fig. 3d, e). Moreover, spatial representations between correct and error trials were also consistent: a linear classifier trained using neural activity in correct trials was able to successfully decode location from error trials (Fig. 3f and Extended Data Fig. 8). Together, these data suggest that pPCx carries a spatial map of the environment that is relatively stable and persistent across time.

How do representations in pPCx differ from those in the hippocampus? Consistent with the prominent role of hippocampus in spatial navigation, populations of hippocampal CA1 neurons represented odour port location even more robustly than did pPCx neurons but only weakly encoded odour identity (Fig. 2e–i, Extended Data Fig. 5). We examined the spatial distribution of peak firing rates for individual pPCx and CA1 neurons as rats travelled across the maze, excluding the periods of odour sampling and reward consumption (Fig. 3g). Normalized peak firing locations for CA1 neurons were distributed along the length of the maze arm, whereas pPCx neurons had peak firing locations at or near ports (Fig. 3h). Across simultaneously recorded populations, location classification accuracy for CA1 was comparable along the length of the maze arm. By contrast, pPCx location-decoding accuracy increased with proximity to ports (Fig. 3i).

Coupling of PCx to the hippocampus

We tested whether odour or location selectivity of pPCx neurons could occur owing to differences in their functional connectivity to bottom-up sensory drive versus top-down hippocampal network activity, as

indexed by synchrony (coherence) of pPCx spikes to either sniffing or hippocampal theta oscillations³⁵ (CA1-LFP), respectively (Fig. 4a). Sniffing frequency characteristically increased during odour sampling³⁶ (Fig. 4a, top, and Extended Data Fig. 9a, b). Location-decoding accuracy (Fig. 4b, bottom) was selectively correlated with the strength of coherence to hippocampal theta and not with sniffing (Fig. 4c, bottom row). By contrast, odour-decoding accuracy (Fig. 4b, top) was robustly correlated with the neurons' coherence to sniff (Fig. 4c, top). Of note, odour-decoding accuracy was also correlated with CA1-LFP coherence during odour sampling, potentially owing to the transient synchrony between sniffing and hippocampal theta band around odour sampling (Extended Data Fig. 9c). The coupling of location-selective cells to hippocampal theta and odour-selective cells to sniffing was reproduced in an analysis of the difference in coherence for the best odour-decoding versus the best location-decoding neurons (Extended Data Fig. 10). Consistent with functionally distinct subpopulations of pPCx neurons, we also found that noise correlations were higher within odour- and location-selective subpopulations than between (Extended Data Fig. 11). We interpret these results to suggest that subpopulations of piriform neurons have differential connectivity to either the olfactory bulb or the hippocampal network^{21,37}, as well as stronger within-population coupling. However, given that we observed a spectrum of response properties ranging from purely sensory to strictly spatial, these subpopulations are probably not strictly segregated.

Discussion

We found that populations of pPCx neurons fired in a spatially restricted manner in a task in which rats used odour cues to navigate to associated rewards in a four-arm maze. pPCx neurons more robustly encoded odour and reward port locations than other parts of the maze. Spatial representations in the pPCx resemble cognitive maps, as they preferentially represented port locations in a manner that was independent of immediate sensory drive, choice correctness, or task engagement. A larger number of pPCx neurons were required to decode odour identity compared to what has been reported for aPCx^{3,22,24,38}. pPCx odour coding also showed a relatively slow rise time and long integration time, contrasting sharply with the fast onset and sniff-locked spike times of aPCx neurons³. We interpret these findings as evidence for a

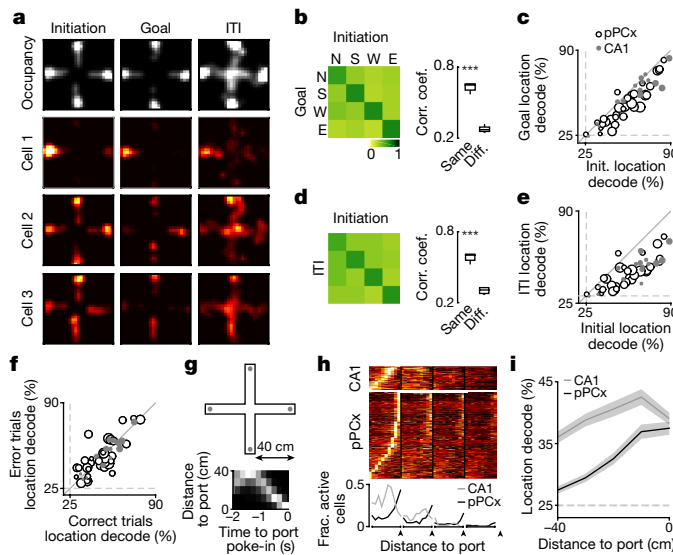


Fig. 3 | Spatial representations are robust and stable across task events.

a, Normalized occupancy of rat on maze and firing-rate heat maps of example cells during three behavioural epochs. Heat maps are plotted using the same colour range across epochs. Peak firing rates (Hz) for cells 1–3: 6.8, 4.8 and 4.3. ITI, intertrial interval. **b**, Pearson's correlation performed on population response vectors at port locations for all location-selective neurons. $n=395$ pPCx cells. The correlation coefficients for visits to the same port (diagonal elements, 'Same': 0.63 ± 0.04) were significantly higher than for visits to different ports (off-diagonal, 'Diff.': 0.28 ± 0.03). Wilcoxon rank-sum test, $P < 0.001$. **c**, Linear classifiers trained on neural responses during the initiation epoch successfully decode location from neural responses during the goal epochs. Cross-validated; chance, 25%. pPCx: $n=33$ sessions, 8–53 cells per session; CA1: $n=15$ sessions, 3–14 cells per session. Init., initiation. Each data point represents a single session. The sizes of data points reflect the number of simultaneously recorded neurons. **d**, **e**, Same analysis as in **b**, **c**, but between initiation and ITI epochs. Wilcoxon rank-sum test, $P < 0.001$. **f**, Linear classifiers trained on activity in correct trials successfully decode location from activity during error trials. **g**, Top, schematic of maze dimensions. Bottom, normalized occupancy histogram of time versus distance from port. **h**, Firing location of CA1 and pPCx neurons along four arms of the maze. x-axis range: -40 to 0 cm. Arrowheads show port locations. The y-axis is sorted by the peak firing location of each neuron on their best arm. Neurons with a place field (peak firing rate greater than $2 \times$ mean rate) anywhere on the maze were included (bottom, $n=468$ pPCx cells and 71 CA1 cells). **i**, Fraction of correctly decoded trials along the length of the maze arm. Cross-validated: chance, 25%. pPCx: $n=33$ sessions, 8–53 cells per session; CA1: $n=15$ sessions, 3–14 cells per session.

functional distinction between these two regions of piriform, where pPCx is comparatively less dedicated to odour coding. However, since learning and behavioural demands may shape brain computation, we speculate that given a more dynamic and complex olfactory environment pPCx could become more engaged in odour coding.

The coupling of pPCx neurons to sniffing rhythms and CA1-LFP reflects the convergence of bottom-up sensory versus top-down cognitive drive. This convergence probably results in the functional heterogeneity of pPCx neurons: neurons range from purely odour-selective and sniffing-coupled neurons to spatially selective and theta-coupled. Neurons with dual odour- and spatial-selectivity, presumably receiving converging bottom-up and top-down information, are well-positioned to connect transient sensory cues to spatial goals during navigation. Future studies on the distinct functions of aPCx and pPCx, as well as subregions of olfactory cortex outside of piriform cortex such as the anterior olfactory nucleus and olfactory tubercle^{32,39} will be important for a more comprehensive understanding of how olfactory and spatial information integrate throughout these neural pathways and the

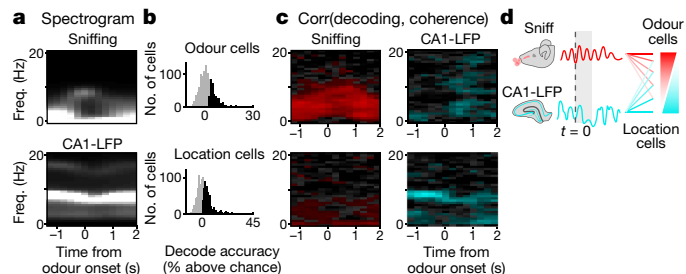


Fig. 4 | Location neurons are coupled to hippocampal theta rhythms.

a, Average spectrogram of sniffing (top) and CA1-LFP (bottom) aligned to odour onset. Brightness indicates power (range 0–90th percentile). **b**, Decoding performance of individual pPCx neurons for odour (top) and location (bottom). Significance was defined as accuracy greater than the 95th percentile of classifiers trained on shuffled labels. **c**, Top, correlation between odour-decoding performance and coherence of spikes to sniffing (left) and CA1-LFP (right). Coloured pixels indicate frequency-time bins in which decoding performance was significantly correlated with sniffing (red) and CA1-LFP (cyan). The coherograms of cells identified as significantly odour coding (**b**) were taken, and for each (time, frequency) value of the coherogram, the across-cell correlation between coherence and decoder was calculated. To identify (time, frequency) pairs with a significant association between decoding and coherence, the correlation was repeated 1,000 times using shuffled decoder values, and (time, frequency) pairs whose value exceeded the 95th percentile were coloured red (for sniff) and cyan (for CA1-LFP). Greyscale range: 0–0.4. y-axis frequency range: 0–20 Hz. Bottom, similar analysis as **c**, top, but for location-decoding accuracy. **d**, Schematic showing preferential coupling between odour and location cells to sniffing and CA1-LFP, respectively.

distinct roles of olfactory and spatial regions engaged during olfactory learning and navigation⁴⁰.

How could piriform spatial maps be generated? We note that whereas projections from hippocampus to piriform cortex are weak, projections from medial and lateral entorhinal cortices^{41–44} provide a direct pathway for top-down influence on the piriform. Piriform circuit features are characteristic of learning systems^{11,17–19}, and active local mechanisms within piriform probably work in concert with top down projections^{21,41,44} to give rise to the spatial representations that we observed. Indeed, whereas firing fields of CA1 place cells tile the length of the maze arm, spatially informative pPCx neurons cluster around port locations. This is consistent with features of a learned spatial map and suggests underlying associative mechanisms for the formation of these spatially restrictive firing fields. Given that in our task water rewards were delivered at the same location as odours, it is not clear whether clustering of spatial representations at ports reflects purely odour-place associations or whether rewards also contribute to map formation.

Cognitive maps are internal models used to represent predictable structures in the world based on an animal's prior knowledge^{33,45}. Animals can produce adaptive and flexible behaviour by combining incoming sensory evidence with cognitive maps of the environment³⁴. Neurons in the hippocampus respond to sensory cues^{46–48}—including odours^{46,49,50}—and sensory cues can also induce global firing rate changes in hippocampal representations referred to as 'remapping'^{51,52}. The encoding of space in piriform illustrates that abstract cognitive variables can be prominently encoded by sensory regions outside of the canonical circuits for spatial cognition^{53–55}. We speculate that whereas the hippocampal formation provides a complete and continuous cognitive map of the spatial environment that is modulated by sensory input^{34,48}, pPCx learns to represent select locations in the environment relevant for olfactory-driven behaviours^{18–20,25,29,38,56}. These findings provide a new avenue of inquiry into the fundamental question of how sensory information is combined with cognitive maps in the brain to guide flexible behaviours.

Online content

Any methods, additional references, Nature Research reporting summaries, source data, extended data, supplementary information, acknowledgements, peer review information; details of author contributions and competing interests; and statements of data and code availability are available at <https://doi.org/10.1038/s41586-021-04242-3>.

1. Baker, K. L. et al. Algorithms for olfactory search across species. *J. Neurosci.* **38**, 9383–9389 (2018).
2. Jacobs, L. F. From chemotaxis to the cognitive map: the function of olfaction. *Proc. Natl Acad. Sci. USA* **109**, 10693–10700 (2012).
3. Miura, K., Mainen, Z. F. & Uchida, N. Odor representations in olfactory cortex: distributed rate coding and decorrelated population activity. *Neuron* **74**, 1087–1098 (2012).
4. Poo, C. & Isaacson, J. S. Odor representations in olfactory cortex: ‘sparse’ coding, global inhibition, and oscillations. *Neuron* **62**, 850–861 (2009).
5. Illig, K. R. & Haberly, L. B. Odor-evoked activity is spatially distributed in piriform cortex. *J. Comp. Neurol.* **457**, 361–373 (2003).
6. Haberly, L. B. Single unit responses to odor in the prepiriform cortex of the rat. *Brain Res.* **12**, 481–484 (1969).
7. Rennaker, R. L., Chen, C.-F. F., Ruyle, A. M., Sloan, A. M. & Wilson, D. A. Spatial and temporal distribution of odorant-evoked activity in the piriform cortex. *J. Neurosci.* **27**, 1534–1542 (2007).
8. Stettler, D. D. & Axel, R. Representations of odor in the piriform cortex. *Neuron* **63**, 854–864 (2009).
9. Gire, D. H., Kapoor, V., Arrighi-Allisan, A., Seminara, A. & Murthy, V. N. Mice develop efficient strategies for foraging and navigation using complex natural stimuli. *Curr. Biol.* **26**, 1261–1273 (2016).
10. Eichenbaum, H. Using olfaction to study memory. *Ann. NY Acad. Sci.* **855**, 657–669 (1998).
11. Johnson, D. M. G., Illig, K. R., Behan, M. & Haberly, L. B. New features of connectivity in piriform cortex visualized by intracellular injection of pyramidal cells suggest that ‘primary’ olfactory cortex functions like ‘association’ cortex in other sensory systems. *J. Neurosci.* **20**, 6974–6982 (2000).
12. Franks, K. M. et al. Recurrent circuitry dynamically shapes the activation of piriform cortex. *Neuron* **72**, 49–56 (2011).
13. Hagiwara, A., Pal, S. K., Sato, T. F., Wienisch, M. & Murthy, V. N. Optophysiological analysis of associational circuits in the olfactory cortex. *Front. Neural Circuits* **6**, 18 (2012).
14. Hasselmo, M. E. & Bower, J. M. Afferent and association fiber differences in short-term potentiation in piriform (olfactory) cortex of the rat. *J. Neurophysiol.* **64**, 179–190 (1990).
15. Poo, C. & Isaacson, J. S. A major role for intracortical circuits in the strength and tuning of odor-evoked excitation in olfactory cortex. *Neuron* **72**, 41–48 (2011).
16. Haberly, L. B. & Price, J. L. Association and commissural fiber systems of the olfactory cortex of the rat. I. Systems originating in the piriform cortex and adjacent areas. *J. Comp. Neurol.* **178**, 711–740 (1978).
17. Haberly, L. B. & Bower, J. M. Olfactory cortex: model circuit for study of associative memory? *Trends Neurosci.* **12**, 258–264 (1989).
18. Hasselmo, M. E. & Linster, C. In *Models of Cortical Circuits* (eds Ulinski, P. S. et al.) 525–560 (Springer, 1999).
19. Barkai, E., Bergman, R. E., Horwitz, G. & Hasselmo, M. E. Modulation of associative memory function in a biophysical simulation of rat piriform cortex. *J. Neurophysiol.* **72**, 659–677 (1994).
20. Haberly, L. B. Parallel-distributed processing in olfactory cortex: new insights from morphological and physiological analysis of neuronal circuitry. *Chem. Senses* **26**, 551–576 (2001).
21. Wang, L. et al. Cell-type-specific whole-brain direct inputs to the anterior and posterior piriform cortex. *Front. Neural Circuits* <https://doi.org/10.3389/fncir.2020.00004> (2020).
22. Bolding, K. A. & Franks, K. M. Complementary codes for odor identity and intensity in olfactory cortex. *eLife* **6**, e22630 (2017).
23. Roland, B., Deneux, T., Franks, K. M., Bathellier, B. & Fleischmann, A. Odor identity coding by distributed ensembles of neurons in the mouse olfactory cortex. *eLife* **6**, e26337 (2017).
24. Iurilli, G. & Datta, S. R. Population coding in an innately relevant olfactory area. *Neuron* **93**, 1180–1197.e7 (2017).
25. Calu, D. J., Roesch, M. R., Stalnaker, T. A. & Schoenbaum, G. Associative encoding in posterior piriform cortex during odor discrimination and reversal learning. *Cereb. Cortex* **17**, 1342–1349 (2007).
26. Haddad, R. et al. Olfactory cortical neurons read out a relative time code in the olfactory bulb. *Nat. Neurosci.* **16**, 949–957 (2013).
27. Zelano, C., Mohanty, A. & Gottfried, J. A. Olfactory predictive codes and stimulus templates in piriform cortex. *Neuron* **72**, 178–187 (2011).
28. Howard, J. D., Plailly, J., Grueschow, M., Haynes, J.-D. & Gottfried, J. A. Odor quality coding and categorization in human posterior piriform cortex. *Nat. Neurosci.* **12**, 932–938 (2009).
29. Wang, D. et al. Task-demand-dependent neural representation of odor information in the olfactory bulb and posterior piriform cortex. *J. Neurosci.* **39**, 10002–10018 (2019).
30. Lak, A. et al. Reinforcement biases subsequent perceptual decisions when confidence is low, a widespread behavioral phenomenon. *eLife* **9**, e49834 (2020).
31. Wallace, D. G., Gorny, B. & Whishaw, I. Q. Rats can track odors, other rats, and themselves: implications for the study of spatial behavior. *Behav. Brain Res.* **131**, 185–192 (2002).
32. Millman, D. J. & Murthy, V. N. Rapid learning of odor-value association in the olfactory striatum. *J. Neurosci.* **40**, 4335–4347 (2020).
33. Tolman, E. C. Cognitive maps in rats and men. *Psychol. Rev.* **55**, 189 (1948).
34. O’Keefe, J. & Nadel, L. *The Hippocampus as a Cognitive Map* (Clarendon Press, 1978).
35. O’Keefe, J. & Recce, M. L. Phase relationship between hippocampal place units and the EEG theta rhythm. *Hippocampus* **3**, 317–330 (1993).
36. Kepcs, A., Uchida, N. & Mainen, Z. F. Rapid and precise control of sniffing during olfactory discrimination in rats. *J. Neurophysiol.* **98**, 205–213 (2007).
37. Martin, C., Beshele, J. & Kay, L. M. An olfacto-hippocampal network is dynamically involved in odor-discrimination learning. *J. Neurophysiol.* **98**, 2196–2205 (2007).
38. Schoonover, C. E., Ohashi, S. N., Axel, R. & Fink, A. J. P. Representational drift in primary olfactory cortex. *Nature* **594**, 541–546 (2021).
39. Agrabawi, A. J. & Kim, J. C. Hippocampal projections to the anterior olfactory nucleus differentially convey spatiotemporal information during episodic odour memory. *Nat. Commun.* **9**, 2735 (2018).
40. Igarashi, K. M., Lu, L., Colgin, L. L., Moser, M.-B. & Moser, E. I. Coordination of entorhinal-hippocampal ensemble activity during associative learning. *Nature* **510**, 143–147 (2014).
41. Agster, K. L. & Burwell, R. D. Cortical efferents of the perirhinal, postrhinal, and entorhinal cortices of the rat. *Hippocampus* **19**, 1159–1186 (2009).
42. Chapuis, J. et al. Lateral entorhinal modulation of piriform cortical activity and fine odor discrimination. *J. Neurosci.* **33**, 13449–13459 (2013).
43. Allen Institute for Brain Science. *Allen Mouse Brain Connectivity Atlas* <https://connectivity.brain-map.org/> (2011).
44. Insaurieta, R., Herrero, M. T. & Witter, M. P. Entorhinal cortex of the rat: cytoarchitectonic subdivisions and the origin and distribution of cortical efferents. *Hippocampus* **7**, 146–183 (1997).
45. Stachenfeld, K. L., Botvinick, M. M. & Gershman, S. J. The hippocampus as a predictive map. *Nat. Neurosci.* **20**, 1643–1653 (2017).
46. Anderson, M. I. & Jeffery, K. J. Heterogeneous modulation of place cell firing by changes in context. *J. Neurosci.* **23**, 8827 (2003).
47. Moita, M. A. P., Rosis, S., Zhou, Y., LeDoux, J. E. & Blair, H. T. Hippocampal place cells acquire location-specific responses to the conditioned stimulus during auditory fear conditioning. *Neuron* **37**, 485–497 (2003).
48. Knierim, J. J. Dynamic interactions between local surface cues, distal landmarks, and intrinsic circuitry in hippocampal place cells. *J. Neurosci.* **22**, 6254–6264 (2002).
49. Radvansky, B. A. & Dombek, D. A. An olfactory virtual reality system for mice. *Nat. Commun.* **9**, 839 (2018).
50. Fischler-Ruiz, W. et al. Olfactory landmarks and path integration converge to form a cognitive spatial map. *Neuron* [10.1101/2021.09.05.552000](https://doi.org/10.1101/2021.09.05.552000) (2021).
51. Muller, R. U. & Kubie, J. L. The effects of changes in the environment on the spatial firing of hippocampal complex-spike cells. *J. Neurosci.* **7**, 1951–1968 (1987).
52. Moita, M. A. P., Rosis, S., Zhou, Y., LeDoux, J. E. & Blair, H. T. Putting fear in its place: remapping of hippocampal place cells during fear conditioning. *J. Neurosci.* **24**, 7015–7023 (2004).
53. Saleem, A. B., Diamanti, E. M., Fournier, J., Harris, K. D. & Carandini, M. Coherent encoding of subjective spatial position in visual cortex and hippocampus. *Nature* **562**, 124–127 (2018).
54. Town, S. M., Brimijoin, W. O. & Bizley, J. K. Egocentric and allocentric representations in auditory cortex. *PLoS Biol.* **15**, e2001878 (2017).
55. Fiser, A. et al. Experience-dependent spatial expectations in mouse visual cortex. *Nat. Neurosci.* **19**, 1658–1664 (2016).
56. Choi, G. B. et al. Driving opposing behaviors with ensembles of piriform neurons. *Cell* **146**, 1004–1015 (2011).

Publisher’s note Springer Nature remains neutral with regard to jurisdictional claims in published maps and institutional affiliations.

© The Author(s), under exclusive licence to Springer Nature Limited 2021

Article

Methods

Animals

A total of 6 male adult Long-Evans hooded rats (4–6 months and weighing 450–550 g) were used in experiments. All 6 rats were used for behavioural analysis (Fig. 1); 3 rats were implanted for neural recordings (Figs. 2–4 and all Extended Data figures). Performance criteria of more than 70% and more than 200 trials per session were reached after approximately 3 weeks of training. Sample size was not predetermined; we established that our sample sizes were sufficient from the size and statistical significance of the effects. Randomization is not relevant to this study as comparisons were not made across groups. Blinding is not relevant to this study as manual curation of single-unit templates was done without knowledge of stimulus responsiveness, and behaviour was analysed automatically without manual scoring.

Odour-cued spatial navigation task

Rats were trained and tested on an odour-cued four-alternative spatial choice task where water was used as a reward based on tasks previously described⁵⁷. Here, rats were trained on an elevated plus maze with open arms and a 25-mm ledge. At the end of each arm there was one nose port which could deliver a light cue, odours, or water reward (modified from Island Motion)⁵⁸. Each odour was associated with one possible reward location (north, south, west or east) (Fig. 1a–c), each trial followed the structure of initiation/odour delivery, navigation, and reward. A trial begins with a light cue indicating the initiation port for that trial. Rats initiated a trial by nose-poking at the port indicated by a light cue. This triggered the delivery of an odour with a (uniform) random delay of 0.1–0.25 s. If rats withdrew their noses before the end of the random delay period, no odours were delivered (short-poke trial). Initiation port location was pseudo-randomized within ten trial blocks and balanced across all port locations; this was critical in animals adopting a location-based (allocentric) rather than direction-based (egocentric) action rule for each odour depending on where it was sampled⁵⁹.

Rats were trained to stay in the odour sampling port for a minimum of 0.15 s, after which they were free to leave (Extended Data Fig. 2a). Odour delivery was terminated as soon as the rat exited the odour port. Following poke-out of the initiation port, a minimum 1.5 s time delay for choice/navigation is enforced to discourage rats from their preference to stay at their current location to collect reward (Extended Data Fig. 2b). After this delay period, water reward is available at the correct port location. A poke in the correct location would yield a tone (80 ms 3 kHz) and a 30-μl water reward while a poke in an incorrect port would yield an error tone (80 ms white noise burst). A 4–6 s (uniform distribution) ITI period started after the delivery of the reward. Reward was available for correct choices for up to 10 s after the rat left the odour sampling port. Water was delivered with a random delay from entry into the goal port drawn from a uniform distribution of 0.5–1.0 s.

The task was designed and implemented using a real-time Linux finite-state machine (RTLFSM) and B-control as described previously⁵⁷. A Point Gray Flea3 1.3MP camera was used to track the rat's behaviour. The Bonsai framework⁶⁰ was used to interface with the cameras.

Odour stimuli

Odour delivery was controlled by a custom made olfactometer⁵⁷ calibrated by a photoionization detector (miniPID, Aurora Scientific). We used relatively low concentration of odourants (liquid dilution factor: 1:100 in mineral oil and further diluting 100 ml min⁻¹ odourized air in a total of 1,000 ml min⁻¹ clean air stream). All odour stimuli (1-hexanol, caproic acid, R-limonene and amyl acetate) were randomly interleaved during a session.

Training

Rats had free access to food, but water was restricted to the training sessions and 5–10 additional minutes of free access per day. Rats were trained in 45-min sessions, twice a day, 5–7 days per week. Each training

session was spaced 6–8 h apart for motivation. To prevent over-training, in 20% of trials (pseudo-randomly interleaved), the correct choice is indicated by a light cue at the correct goal port (answer trials). In the remaining 80% of trials, all 4 possible goal ports are lit (question trials). A threshold of 75% correct for question trials (chance is 25%) is taken as performance criterion. All behavioural and neural data analysis were restricted to question trials only.

Microdrive implant

After reaching an asymptotic performance in behavioural training, each rat was implanted with a custom-designed and 3D printed multielectrode drive (based on microdrives designed in the laboratory of L. M. Frank at UCSF) (PolyJetHD Blue, Stratasys) with 24 independently moveable tetrodes (based on design from the laboratory of L. M. Frank at UCSF). Tetrodes (Ni-Cr, California Fine Wire Company) were arranged into a 3 × 8 array within a cannula and gold plated to reach an impedance of 250 kΩ at 1 kHz. Implanted recording drives had two cannulas that targeted both pPCx (19 tetrodes, rectangular cannula angled at 19 degrees coronal angle away from the midline), and dorsal CA1 (5 tetrodes, vertical cannula). Cannulas were centred at the following coordinates: right pPC –2.0 mm AP and 3.0 mm ML, right dorsal hippocampal CA1 –4.2 mm AP and 2.0 mm ML. LEDs were attached to the microdrive and used for video tracking of rat position.

Neural recordings

After 10 days of post-operative care and recovery, rats were water restricted and trained in the same manner as the pre-surgery period. Tetrodes were adjusted every 2 days post-surgery to reach the target coordinate, guided by depth, LFP and spiking patterns. Before starting recordings, animals were retrained to reach similar accuracy levels as those achieved before surgery (>75% correct for question trials). Recording sessions were split into two 45-min behavioural blocks with a 15–20 min rest period in between blocks to allow for rats to rest and consume food in a separate box. During this time, surfaces of the maze and port were cleaned thoroughly with enzymatic cleaner (Henry Schein Medical) and disinfectant (VirkonTM-S, and 70% ethanol). Electrical signals were amplified and recorded using the Cerebus data acquisition system (Blackrock Microsystems). Thresholded events were recorded at 20 kHz (for spike sorting), continuous signal was recorded at 2 kHz (for LFP). Due to the large distance between tetrode entry point and target piriform cell body later, in order to target piriform primary cell body layer, a single tetrode in the most anterior position was advanced ahead of the rest ('scout' tetrode), past the entire principal cell body layer (as identified by increases in threshold-crossing events), to reach the ventral lateral inner surface of the cranium (as identified by a signature pop of voltage saturation followed by complete lack of threshold-crossing events). The remaining tetrodes were then advanced to the cell body layer depth as identified by the 'scout' tetrode, while taking into account the medial-lateral inclination of cell body layer depth. Tetrode depths were adjusted at the end of each session while monitoring spike waveform and firing properties in order to sample an independent population of neurons across sessions. The locations of tetrode tips during each recording session were estimated based on their depth and histological examination based on electrolytic lesions and the visible tetrode tracks. Rats performed 1 session per day, and a total of 44 recording sessions were obtained from 3 rats.

Recording and analysis of respiration pattern

To monitor sniffing, during drive implantation, a temperature sensor (custom T-type probe, 44 gauge, Physitemp Instruments) was implanted in one nostril, and respiration patterns were monitored as a temperature change in the nasal cavity as described previously⁵⁷. Signals from nasal thermocouple were amplified, filtered between 0.1 and 475 Hz and digitized at 2,000 Hz. For analysis, voltage signals were further low-pass filtered (< 50 Hz). Onset of inhalations and

exhalations were identified as local maxima and minima of the signals semi-automatically using custom software.

Histology

To verify the ultimate location of the tetrodes, electrolytic lesions were produced after the final recording session ($30\text{ }\mu\text{A}$ of cathodal current, 3 s). Rats were deeply anesthetized with pentobarbital and perfused transcardially with 4% paraformaldehyde (wt/vol in PBS). The brain was sectioned at $50\text{ }\mu\text{m}$ and stained with Cresyl violet solution to observe sites of electrolytic lesions (Extended Data Fig. 1).

Data analysis and statistics

All data analysis and statistical tests were performed with custom-written software using MATLAB (Mathworks). No statistical methods were used to pre-determine sample sizes.

Behavioural bias analysis. Fig. 1f, g: Delta bias is the change in probability of choosing a particular location in the next trial as a consequence of the outcome of the current trial. We can express this as:

$$\begin{aligned}\Delta\text{Bias}(\text{Loc}_{t-1}, \text{Loc}_t, \text{Loc}_{t+1}, R_t) \\ = P(\text{Loc}_{t+1}|\text{Loc}_t, R_t) - P(\text{Loc}_{t-1}|\text{Loc}_t, R_t)\end{aligned}$$

Where t is the current trial; location $\text{Loc} \in \{\text{north, south, west, east}\}$ and reward $R \in \{0, 1\}$. The location bias (LocBias) is defined as the delta bias of repeating the same location and results from fixing the location and conditioning the analysis to rewarded and non-rewarded trials:

$$\text{LocBias}(R) = \sum_t^{\text{Loc}} \Delta\text{Bias}(l, l, l, R)$$

The same analysis was performed for actions by substituting Loc for Action $\in \{\text{left, right, forward, stay}\}$.

Spike sorting. Single units were isolated offline by manually clustering spike features derived from the waveforms using spike-sorting software provided by D. N. Hill, S. B. Mehta and D. Kleinfeld⁶¹. Single-units recorded on more than one session, as judged from the spike waveform and the firing pattern, were excluded from the analysis, but the results were not affected by the inclusion of all units. Recordings from outside the pPCx or CA1 were excluded from the analysis. We also excluded units with <200 spikes in a given session. As in other cortical areas, neurons could be classified into two categories: wide-spiking (width > 0.2 ms) and narrow-spiking neurons (width < 0.2 ms). The width was determined as the time between a peak and a trough of the mean spike waveform. About 4% (39) of recorded neurons fell into the category of narrow-spiking neurons. Overall, pPC neurons had spontaneous firing rates of 2.79 ± 3.74 Hz (mean \pm s.d.). Spontaneous firing rates of wide-spiking neurons were significantly lower than those of narrow-spiking neurons (2.23 ± 2.49 Hz; 16.41 ± 3.43 Hz; mean \pm s.d.). Both categories of cells were included in the analyses but exclusion of narrow spike neurons did not affect the main conclusions.

Single-neuron responsiveness and selectivity analysis. In order to obtain instantaneous firing rates (for example, for peri-event time histograms (PETHs)), spike events were convolved with a Gaussian filter (s.d.: 25 ms). Odours: to identify odour responsive neurons (for example, Extended Data Fig. 4d), we compared the firing rate of a 1 s time window after odour onset to a 1 s time window immediately prior to odour onset using the Wilcoxon rank sum test, $P < 0.01$. To identify neurons that were odour-selective (for example, Fig. 2e) we compared the firing rate during a 1 s time window after odour onset across the four odour stimuli using an ANOVA test, $p < 0.01$. Locations: location selectivity of individual neurons was obtained from comparing firing rates in 20×20 cm position bins centred around individual port locations on

maze using ANOVA test, $P < 0.01$ (see ‘Analysis of firing rate on maze’). Odour and location responses in example session (Fig. 2d): z-scored firing rate of neurons for odours were taken between 0–1 s after odour onset. Mean z-scored firing rate for locations was calculated from occupancy normalized firing rate heat map, using $20\text{ cm} \times 20\text{ cm}$ position bins centred around port locations.

Analysis of firing rate on maze. For firing rate heat map visualization (Figs. 2, 3, Extended Data Figs. 3, 8b), rat positions (tracked by LED on the microdrive) on the maze ($1\text{ m} \times 1\text{ m}$) was divided into 4×4 cm bins. Mean firing rate for each position bin normalized by occupancy was obtained and then smoothed with a gaussian kernel (s.d.: 2 cm). Responses for each neuron used for location selectivity and correlation analysis was obtained by dividing the maze into 20×20 cm bins. The mean z-scored firing rate for the position bin centred on each port was taken as response at a particular location. Firing rate heat maps for individual odours (Fig. 2a–c) were obtained by sorting trials by odour identity, and obtaining the firing rate heat map for all concatenated trials of the same odour.

Firing rate heat maps for the three behavioural epochs (Fig. 3a, initiation, goal and ITI) where taken from all trials within a session and concatenated. Initiation epoch is –0.5 to 0.5 s around initiation port entry. Goal epoch is –0.5 to 0.5 s around goal port entry. ITI starts 1.0 s after goal port entry and has a duration of 4–6 s (randomly drawn from a uniform distribution).

Firing rate heat maps for correct and error trials (Extended Data Fig. 8b) were generated by concatenating trials from –1 to 2 s window around initiation and goal port entry in the entire session. For peak firing location of CA1 (Fig. 3h, top) and pPCx (Fig. 3h, middle) neurons along four arms of the maze, plots were ordered from best to worst. The best arm (left-most plot) was defined as the arm on which neurons had their peak firing plots. Activity was taken during a 2.0 s time window prior to initiation port poke-in (before odour onset) and normalized to peak firing rate on the best arm.

Population correlations. Figs. 2, 3, Extended Data Fig. 5a: Odour: population odour response vectors consisted of mean z-scored firing rate of neurons within a 1-s time window after odour onset. Location: population location response vectors consisted of mean z-scored firing rate on the maze as described above in ‘Analysis of firing rate on maze’. Pearson’s correlation coefficient was used for reported correlation coefficients. Qualitatively similar results were obtained using Spearman’s rank correlation coefficient.

ROC analysis odour. Odour response magnitudes were characterized in terms of how discriminable odour responses are from conditions in which no odours were delivered (short-poke trials) using the ROC analysis^{62,63}. The area under the ROC curve (auROC) for a single neuron characterizes the discriminability of odour trials from no odour trials. We compared neural response 0.25–1.25 s (as shown in Extended Data Fig. 6a) after odour onset in odour trials to a 0–1 s after initiation port poke in no odour (short-poke) trials. We only included windows during which rat position was within the outer 40% of the arm for both odour and no odour trials. This was to control for potential variability in firing rates between odour versus non-odour trials caused by animals being in different locations, given that neurons in pPCx can change their firing rates across locations. Location: to examine how discriminable firing rates at port locations were from firing rates at non-port locations, we compared a 1 s time window immediately prior to odour onset, while rats occupied the outer 40% of the arm (port location), to a 1 s time window leading up to initiation port poke-in in which rats occupied the inner 40% of the arm (non-port location). We only included time periods prior to odour onset for both location and non-port location windows to control for potential variability in firing rates caused by odours.

Article

Sparserness. Extended Data Fig. 4: Population sparseness (S_p) is defined for a given odour using the formula $S_p = \{1 - (\sum r_j/N)^2 / \sum r_j^2/N\} / [1-(1/N)]$, where N is the number of neurons and r_j is the trial-averaged neural response (z-scored firing rate) of each neuron to the given odour^{64,65}. Lifetime sparseness (S_L) is calculated for each neuron using the above formula except j corresponds to each odour and N the total number of odours tested. Accordingly, S_p quantifies sparseness of odour-evoked activity across a population for a given odour (0, uniform; 1, sparse). S_L quantifies sparseness of odour responses (specificity) for a given neuron (0, uniform; 1, sparse). Population and lifetime sparseness for port locations were obtained similarly, using neural responses for port locations instead of odours.

Pseudopopulation decoding. Subsets of neurons were sampled from across recording sessions. Population sizes were sampled at increments of $\sqrt{2}$ up to the total number of available neurons leading to pseudopopulations of 2–725 (pPCx) and 2–91 (CA1). Neuronal responses were concatenated into a matrix, arranged so that each row contained responses to a particular (odour–location). Because different sessions contained different numbers of trials, a random subset of responses from each neuron was excluded so that the number of trials per category was consistent across neurons in the pseudopopulation. For each population size, the sampling procedure was repeated ten times. Each neuron's response was averaged over a 1-s window whose timing was chosen to maximize population decoding (see Extended Data Fig. 5; 0.25–1.25 s post-odour onset for odour decoding; −0.5 s to 0.5 s peri-poke in for location decoding). Sniff-aligned odour decoding (Extended Data Fig. 5b) was performed by defining the first inhalation peak post-odour onset as $t = 0$. Each neuron's response was normalized by taking the z-score across all trials. Trials were labelled 1–4 according to the odour sampled (for odour decoding) or port location (for location decoding), and arranged into a T (no. of trials)-element vector. Sessions with fewer than 400 trials per session were excluded, since it would lead to overall fewer usable trials in the entire pseudopopulation analysis. Multi-class classification was performed with the LIBLINEAR library⁶⁶ (<https://www.csie.ntu.edu.tw/~cjlin/liblinear/>), using either L1- or L2-regularized logistic regression with fivefold cross-validation.

Population decoding. For per-session decoding, neuronal firing rates were arranged into a matrix of size T (no. of trials) $\times N$ (no. of neurons). Trials were labelled 1–4 according to the odour sampled (for odour decoding) or port location (for location decoding), and arranged into a T (no. of trials)-element vector. This matrix was normalized by taking the z-score of each column (so that each neuron's firing rate was standardized). The vector of labels and matrix of firing rates were fed into a multi-class L1-regularized logistic regression (LIBLINEAR⁶⁶, see previous section) using fivefold cross validation. Chance-level classification was estimated by running the same classifier on shuffled labels. For decoder time courses (Fig. 2h, l), 200-ms non-overlapping windows were used. For pre-vs-post odour decoding (Extended Data Fig. 7b, c), time windows of 1-s before and after initial poke-in were used. Data sessions with fewer than eight pPCx neurons were excluded because they had substantially fewer simultaneously recorded cells.

Population activity across epochs. Fig. 3a–c: Initiation and goal epochs were defined as 1-s time windows centred around initiation and goal port poke-in times, respectively. ITI epoch was defined as the 4–6 s time window enforced in between trials. Occupancy of rat and firing rate heat maps for temporal epochs (Fig. 3a) were obtained by concatenating time periods of the same epoch.

Classification of location during correct and error trials. Each neuron's average response during the time window −0.5 to 0.5 s peri-initiation port poke-in was concatenated, z-scored across trials, and trained

to classify port location as described in the 'population decoding' section. The trained decoder was used to classify the animal's position during goal port poke-in for either correct or incorrect trials (Fig. 3f). For Extended Data Fig. 8c, the decoder was trained using only peri-initiation port poke-in for correct trials only. Sessions with fewer than 8 simultaneously recorded pPCx neurons were excluded.

Place field distribution along maze arm. Fig. 3h: Each neuron's 'place field' was defined as its mean firing rate in each of ten equally divided sections of each of the four arms of the plus-maze. Data were restricted to the 2-s period preceding poke-in, so that place fields reflected approach to port (and not departure). Neurons whose response along track never exceeded 2× the mean firing were excluded. Results were similar for other thresholds. Neurons were sorted by their place field locations along the arm containing peak response.

Identity decoding along maze arm. Figure 3i: Data were restricted to the 1.5 s period preceding poke-in, which corresponds to the period where the animal is running up the maze arm (Fig. 3g). Neuronal firing rates were sampled at 5 Hz and z-scored, and the rat's position was discretized into 5 equally-spaced bins along the arm length. 5 separate classifications were performed, one for each of the 5 bins, to predict which of the 4 arms the rat was occupying using either populations of simultaneously recorded pPCx or CA1 neurons. As with population decoding, classification was performed using LIBLINEAR⁶⁶ with fivefold cross-validation.

Identification of CA1-LFP. For each rat, the 96-electrode LFP data was represented as a 96-dimensional matrix sampled at 40 Hz. Each row of this matrix (representing a single electrode time series) was high-pass filtered using zero-phase 'filtfilt' function in MATLAB, and a 2-Hz, 2nd order Butterworth filter. The resulting matrix was truncated to include only the time window [−1.5 s, 2 s] around the time of all trial-initiating poke-ins taking place within a session. For a given rat, the procedure was repeated for all sessions, and the resulting matrices were concatenated into a single matrix. In summary, this pre-processing captured each animal's multi-electrode LFP during odour sampling and across sessions. Singular value decomposition (SVD) was applied to the resulting matrix, and the trial-averaged spectrograms (see below) of the top 10 components were visualized. To identify hippocampal theta, we looked for a component with power in the −8 Hz band⁶⁷. For each rat, we picked the highest-variance component of this sort. Two additional lines of evidence suggested that we successfully identified theta: (1) theta power decreased around the time of poke-in, consistent with the observation that theta power decreases during periods of immobility⁶⁷; and (2) the components showed strong coherence with identified hippocampal spiking activity³⁵ at −8 Hz (see Extended Data Fig. 9d, lower right panel).

Spectral analysis. Neural activity across the olfactory-limbic pathway displays dynamical coupling to sniffing or internally generated oscillatory rhythms during behaviour^{3,7,68,69}. To compute power spectra and coherograms (Fig. 4, Extended Data Fig. 9), the Chronux toolbox⁷⁰ was used (<http://chronux.org/>). Each neuron's coherence with sniffing and CA1-LFP was calculated as a function of time and frequency using the function cohgramcpb, using $F_s = 40$ Hz, a sliding window of 1 s with a stride of 0.2 s, and taper set to [1 Hz, 1 s, 1]. Similarly, the power spectrum for sniff and CA1-LFP was calculated using the function specgram, with the same parameter settings. For this and subsequent analysis, data of 1 of 3 rats was excluded because it performed far fewer trials per session, leading to noisy estimates of coherence.

Single-cell decoding. For each neuron, the firing rate was sampled at 2 Hz over the interval [−2 s, 2 s] with respect to initial poke-in (for location classification) and the interval [0 s, 2 s] with respect to odour onset

(for odour classification). This was repeated across all trials, resulting in an R (no. of trials) $\times T$ (no. of time steps) matrix. Each column of the matrix (that is, each time point) was z-scored. Corresponding R-element vectors containing labels for poke-in location and odour identity was defined. For each, a linear multi-class decoder (using LIBLINEAR⁶⁶, see above) was trained to classify odour–location based on the firing rate time series. This procedure was repeated 100 times for label-shuffled data to establish each neuron’s baseline classification performance, which deviated from 25% because of non-uniform trial sampling in sessions. Finally, the mean chance-level performance was subtracted, and neurons whose classification accuracy exceeded the 95th percentile of the baseline classification accuracy were labelled as significant.

Relating single-cell decoding to coherence: correlation between decoding accuracy and coherence. Fig. 4c: The coherograms of cells identified as significantly odour or location coding (see above) were taken, and for each (time, frequency) value of the coherogram, the across-cell correlation between coherence and decoder accuracy was calculated. To identify (time, frequency) pairs with a significant association between decoding and coherence, the correlation was repeated 1,000x using shuffled decoder values, and (T, F) pairs whose value exceeded the 95th percentile were coloured red (for sniff) and blue (for CA1-LFP).

Top n cells analysis. Extended Data Fig. 10: The top n odour- and location-decoding cells were taken from Fig. 4b, and the difference of their mean coherograms was plotted. Significant (T, F) bins were identified as those whose values were significantly higher (lower) between the top n location and top n odour cells were colored blue (red), as indicated by a t -test (ttest2 in MATLAB).

Noise correlation analysis. Extended Data Fig. 11: For each trial, each pPCx neuron’s activity was averaged over the 1-s period preceding poke-in. To remove potential signal correlations related to the animal’s position (odour responses did not apply to this pre-poke period), each neuron’s average response to the port was subtracted from the trial-specific firing rate. This was done separately for the first and second blocks of trials within a session, since the firing rates for some neurons drifted during the gap between trial blocks. Neurons were classified as significantly odour coding (O), significantly location coding (L), or neither. For pairs of neurons belonging to the same session, the Pearson correlation coefficient was calculated and added to one of 6 sets corresponding to all possible pairings between O, N, and L. Note that O–O and L–L could contain the same neurons, since a neuron could be both odour- and location-coding. In contrast, the O–L group contained neurons that were exclusively odour or location coding, respectively. Results were similar when restricting O–O and L–L groups to be exclusively odour- or location-coding, respectively, or when increasing the sampling rate of neuronal firing (up to 16 Hz, the maximum tested).

Reporting summary

Further information on research design is available in the Nature Research Reporting Summary linked to this paper.

Data availability

Data will be made available upon reasonable request to the corresponding authors.

57. Uchida, N. & Mainen, Z. F. Speed and accuracy of olfactory discrimination in the rat. *Nat. Neurosci.* **6**, 1224–1229 (2003).
58. Felsen, G. & Mainen, Z. F. Neural substrates of sensory-guided locomotor decisions in the rat superior colliculus. *Neuron* **60**, 137–148 (2008).
59. Restle, F. Discrimination of cues in mazes: a resolution of the ‘place-vs.-response’ question. *Psychol. Rev.* **64**, 217 (1957).
60. Lopes, G. et al. Bonsai: an event-based framework for processing and controlling data streams. *Front. Neuroinform.* **9**, 7 (2015).
61. Hill, D. N., Mehta, S. B. & Kleinfeld, D. Quality metrics to accompany spike sorting of extracellular signals. *J. Neurosci.* **31**, 8699–8705 (2011).
62. Dayan, P. & Abbott, L. F. *Theoretical Neuroscience: Computational and Mathematical Modeling of Neural Systems* (MIT Press, 2001).
63. Green, D. M., Swets, J. A. et al. *Signal Detection Theory and Psychophysics* Vol. 1 (Wiley, 1966).
64. Rolls, E. T. & Tovee, M. J. Sparseness of the neuronal representation of stimuli in the primate temporal visual cortex. *J. Neurophysiol.* **73**, 713–726 (1995).
65. Willmore, B. & Tolhurst, D. J. Characterizing the sparseness of neural codes. *Network* **12**, 255–270 (2001).
66. Fan, R.-E., Chang, K.-W., Hsieh, C.-J., Wang, X.-R. & Lin, C.-J. LIBLINEAR: a library for large linear classification. *J. Mach. Learn. Res.* **9**, 1871–1874 (2008).
67. Richard, G. R. et al. Speed modulation of hippocampal theta frequency correlates with spatial memory performance. *Hippocampus* **23**, 1269–1279 (2013).
68. Kay, L. M., Beshe, J., Brea, J. & Martin, C. Olfactory oscillations: the what, how and what for. *Trends Neurosci.* **32**, 207–214 (2009).
69. Litaudon, P., Amat, C., Bertrand, B., Vigouroux, M. & Buonviso, N. Piriform cortex functional heterogeneity revealed by cellular responses to odours. *Eur. J. Neurosci.* **17**, 2457–2461 (2003).
70. Mitra, P. & Bokil, H. *Observed Brain Dynamics* (Oxford Univ. Press, 2007).

Acknowledgements We thank J. J. Paton, B. A. Atallah, L. L. Glickfeld and J. B. Hales for comments on the manuscript; members of the Mainen laboratory, E. Lottem, M. Murakami, M. G. Bergomi, C. Linster, M. Moita, A. Fleischmann, K. M. Franks, S. R. Datta, C. E. Schoonover, A. J. P. Fink, and R. Axel for helpful discussions; A. S. Cruz and A. C. Rato for assistance with animal training; L. M. Frank and members of the Frank laboratory for experimental advice and assistance; G. Costa for scientific illustrations; Champalimaud Research Hardware Platform for custom components used in the behavioural task and recordings; and Champalimaud Vivarium Platform for animal care. We acknowledge Champalimaud Foundation (Z.F.M.), European Research Council (Advanced Investigator Grant 671251, Z.F.M.), Human Frontier Science Program (LT0000402/2012, C.P.), Fundação para a Ciéncia e a Tecnologia (FCT-PTDC/MED-NEU/28509/2017, C.P.), and Helen Hay Whitney Foundation (C.P.) for financial support. This work was supported by Portuguese national funds, through Fundação para a Ciéncia e a Tecnologia (FCT)—UIDB/04443/2020, CONGENTO, co-financed by Lisboa Regional Operational Programme (Lisboa2020), and FCT LISBOA-01-0145-FEDER-02210.

Author contributions The project was originally conceptualized by C.P. and Z.F.M. and further developed in collaboration with N.B. The behavioural paradigm was developed and designed by C.P., N.B. and Z.F.M. Task-related hardware was developed and constructed by N.B. and C.P. Task-related software was developed and implemented by N.B. Animal training, behaviour data collection and behavioural data analysis was performed by C.P. Neural recordings were performed by C.P. Neural data analysis was performed by C.P. and G.A. The manuscript was written by C.P., G.A. and Z.F.M. and edited and reviewed by all authors.

Competing interests The authors declare no competing interests.

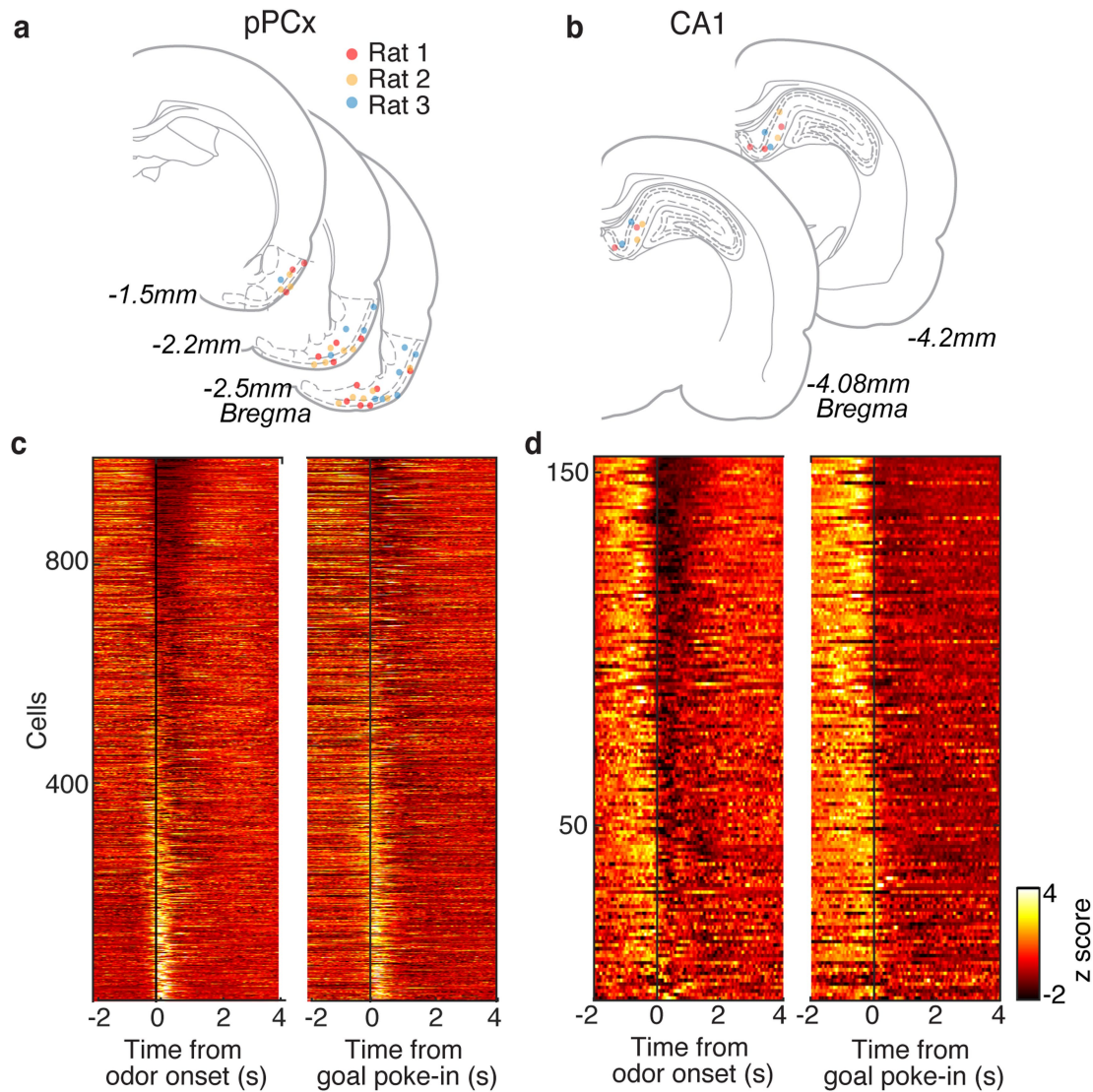
Additional information

Supplementary information The online version contains supplementary material available at <https://doi.org/10.1038/s41586-021-04242-3>.

Correspondence and requests for materials should be addressed to Cindy Poo or Zachary F. Mainen.

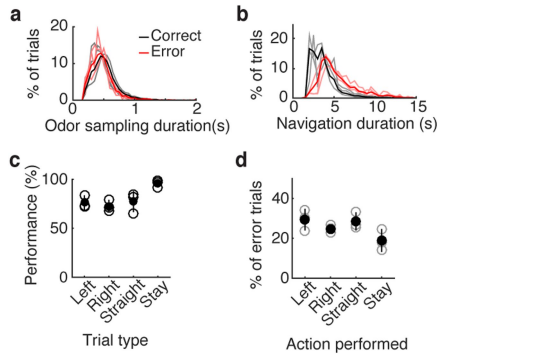
Peer review information *Nature* thanks the anonymous reviewer(s) for their contribution to the peer review of this work.

Reprints and permissions information is available at <http://www.nature.com/reprints>.



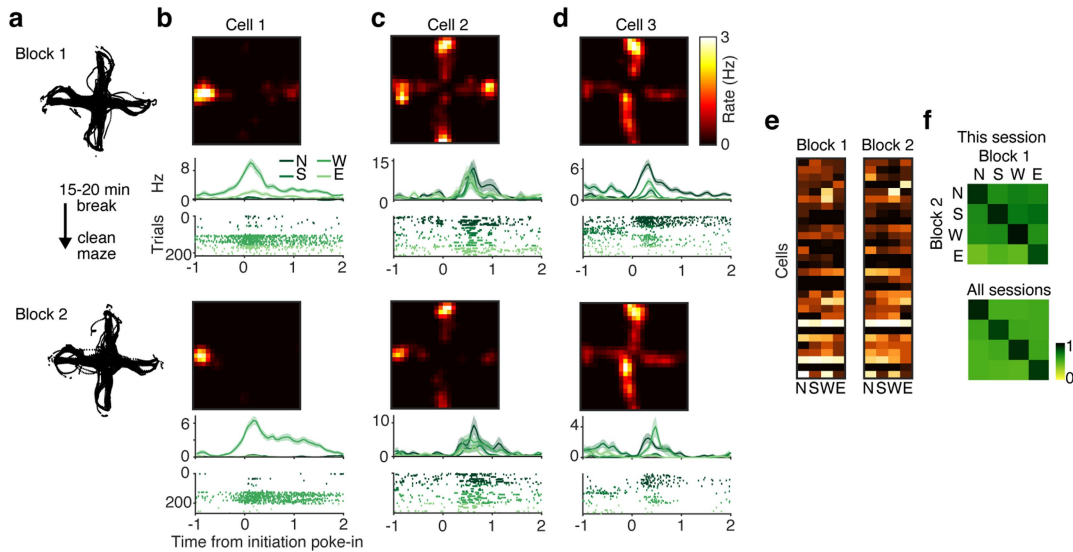
Extended Data Fig. 1 | Tetrode lesion sites and population summary of pPCx and CA1 neurons. (a) Tetrode lesion sites for 3 recorded rats in pPCx. See full methods for targeting and verification of tetrode recording sites. Due to the wide range of tetrode lesion sites (from -1.5 mm to -2.5 mm bregma), lesion sites from multiple histological sections were summarized onto 3 representative atlas sections. (b) Summary PETH for all pPCx ($n=995$) neurons recorded. Spike timing was aligned to odour onset (left) and goal poke-in

(right). Neurons were sorted based on their activity during 1 s time window after odour onset in both left and right panels. For each neuron, the mean z-scored rate during a 2 s time window prior to alignment time point was subtracted from the entire PETH. (c) Tetrode lesion sites for 3 recorded rats in dorsal CA1. See Full Methods for targeting and verification of tetrode recording sites. (d) Summary PETH for all CA1 ($n=154$) neurons recorded.



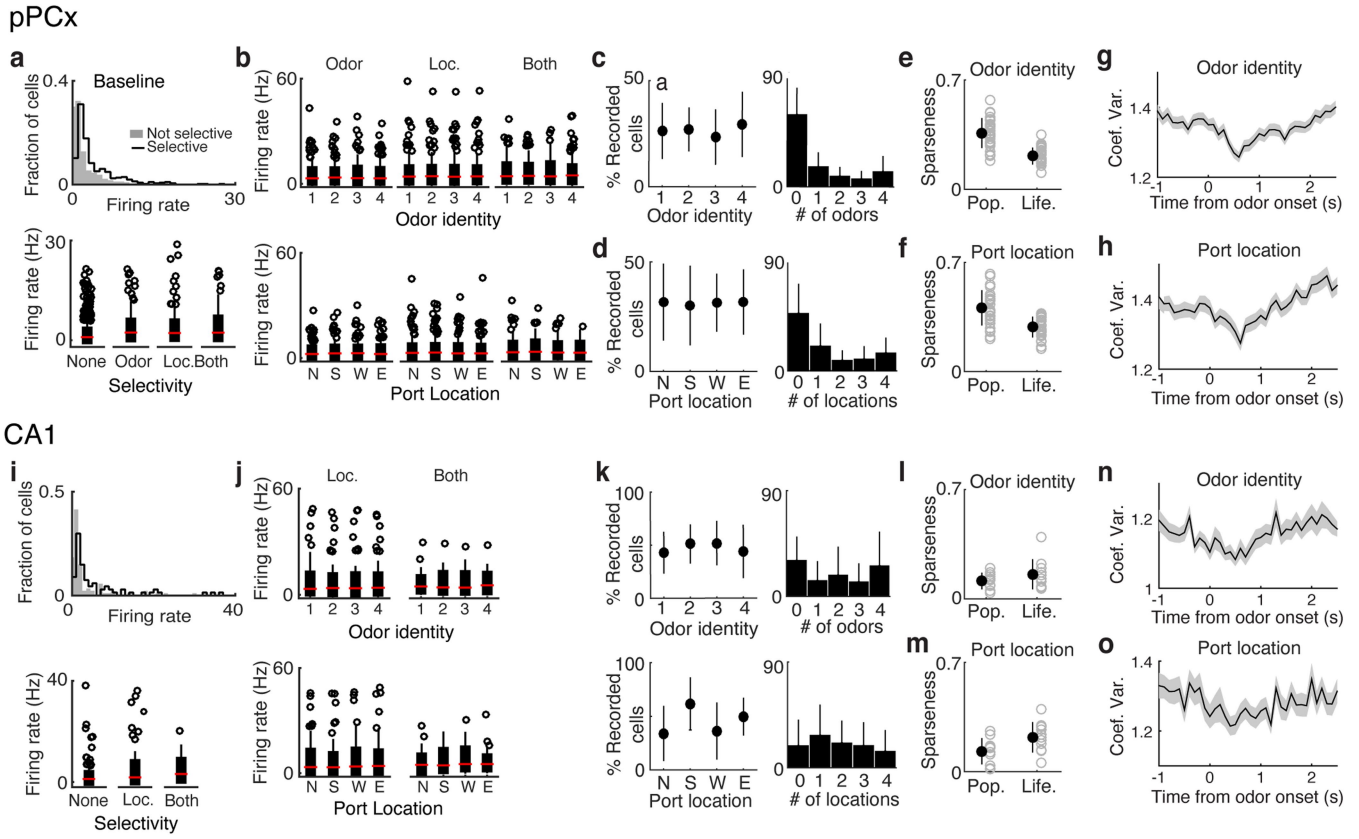
Extended Data Fig. 2 | Correct and error trial behavior in odour-cued spatial choice task.

(a) Odour sampling duration in 3 recorded rats. A minimum of 150 ms of odour sampling was enforced. Black: correct trials, 0.519 ± 0.02 s. Red: error trials, 0.448 ± 0.04 s. **(b)** Navigation duration in 3 recorded rats, as defined by time between initiation (odour) port poke-out and goal port poke-in. Goal ports were only active (reward available) after a 1.5 s delay after rats poke out of initiation ports. Black: correct trials, 3.67 ± 0.15 s. Red: error trials, 5.35 ± 0.8 s. **(c)** Rats performed better for trials in which goal location indicated by the odour cue was congruent with odour sampling location (stay trials). $n = 3$ rats, ANOVA, $p = 0.01$, Mean \pm S.D. **(d)** Actions performed for error trials. ANOVA, $p = 0.07$. Mean \pm S.D.



Extended Data Fig. 3 | pPCx location selectivity remains stable across recording blocks. (a) Rat position on the maze during two blocks within the same recording session. (b-d). Occupancy normalized firing rate heat map, PETH, and raster plots associated with example cells 1-3 in Fig 2a-c. PETH and raster plots were aligned to initiation port poke-in and sorted by location. (e). Z-scored mean firing rate of neurons for different port locations across blocks. (f) Stability of port location representation between the two blocks was calculated the pairwise Pearson's correlation coefficient for population activity across different locations in these two blocks. Values along the diagonal band in the correlation coefficient matrix represent the similarity of the pPCx population response to the same location in two recording blocks.

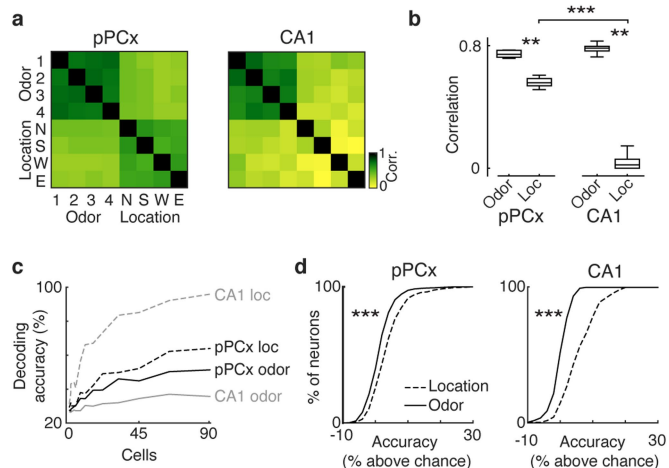
(f, top) Similarity matrix obtained by computing the pairwise Pearson's correlation coefficients between locations population response vectors for blocks 1 and 2 of example session shown in (a-e). Coefficients along the diagonal band are significantly higher than off-diagonal ($r_{\text{diag}} = 0.80 \pm 0.05$, $r_{\text{offdiag}} = 0.54 \pm 0.09$, Wilcoxon rank-sum test, $p < 0.01$), indicating that location representations were stable between blocks. **(f, bottom)**. Same analysis as in the top panel but for all pPCx neurons recorded ($r_{\text{diag}} = 0.81 \pm 0.02$, $r_{\text{offdiag}} = 0.47 \pm 0.02$, Wilcoxon rank sum test, $p < 0.001$, $n = 44$ sessions, 995 neurons). We conclude from these data that uncontrolled odours were unlikely to account for the pPCx location representations observed.



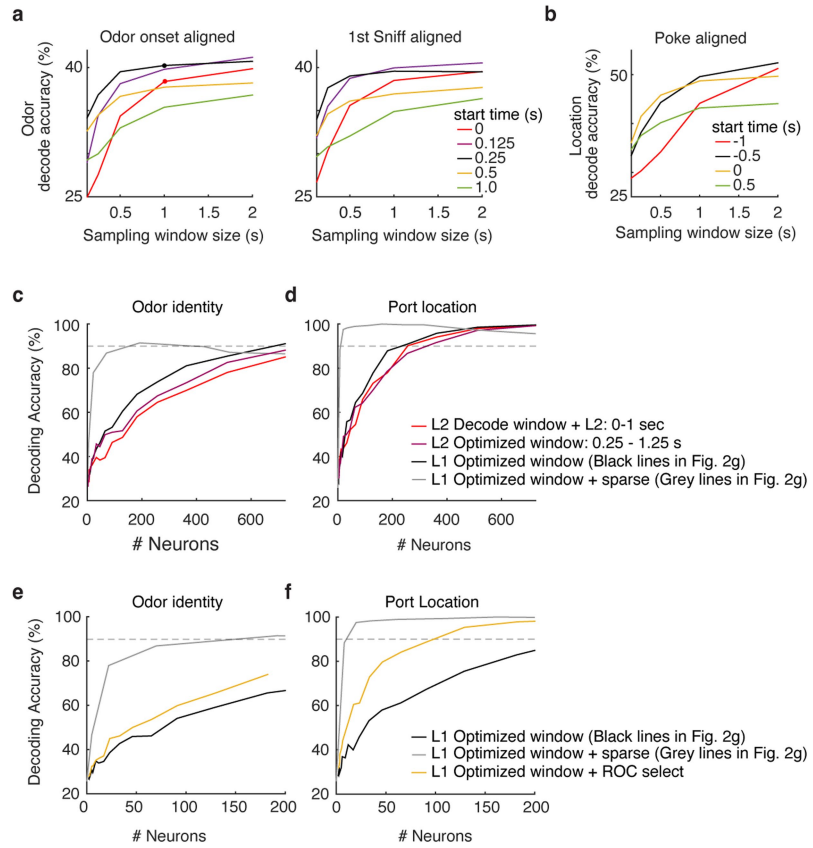
Extended Data Fig. 4 | Summary of pPCx and CA1 response properties for odours and port locations in task. (a, top) Firing rate for individual pPCx neurons throughout recording sessions. Non-selective neurons: median = 0.94, range = 0.03 – 21.48 Hz, n = 531 neurons; selective neurons (for either odour or location): median = 1.95, range = 0.04 – 27.49 Hz, n = 464 neurons. (a, bottom) Firing rate of neurons grouped by selectivity properties. Odour-selective only neurons (Odour), n = 120 neurons, median = 1.93, range = 0.05 – 17.84 Hz. Location-selective only neurons (Loc.), n = 238, median = 2.06, range = 0.04 – 27.49 Hz. Odour and location selective neurons (Both): n = 106, median = 1.88, range = 0.14 – 17.41 Hz. (b, top) Firing rates for individual neurons across 4 odour identities during 0 – 1.0 s post odour onset. Neurons are grouped by selectivity properties. Red tick: median; edges of the bar indicate the 25th and 75th percentiles; circles: outliers. (b, bottom) Same as (b, top) but across port locations. (c, left) Fraction of recorded pPCx neurons in a session that was activated by different odours. Activation was measured by comparing mean firing rate for 1 s after odour onset time compared to a 1 s baseline immediately preceding odour onset (n = 33 sessions). Wilcoxon rank-sum test, p < 0.05, corrected for multiple comparisons (see Full Methods). (c, right) Histogram of number of odours that activate pPCx cells in a session. (d) Similar to (c) but for

port locations. Location selectivity of individual neurons was obtained from comparing firing rates in 20 x 20 cm position bins centered around individual port locations on maze using ANOVA-test, p < 0.01 (e) Sparseness across odour identity for simultaneously recorded populations. Population sparseness = 0.36 ± 0.09 ; lifetime sparseness = 0.21 ± 0.05 , Mean \pm S.D. (n = 33 sessions). (f) Similar to (e) but for port locations. Population sparseness = 0.40 ± 0.12 ; lifetime sparseness = 0.29 ± 0.06 . (g) Coefficient of variation for odours aligned to odour onset. Trial-to-trial coefficient of variation for each neuron was calculated for different odour trials and averaged. (h) Similar to (g) but calculated for different port locations. (i–o) Same analysis as (a–h) for CA1 population. (i, top) Non-selective neurons: median = 1.22, range = 0.12 – 38.15 Hz, n = 88 neurons; selective neurons (for either odour or location): median = 2.35, range = 0.11 – 36.11 Hz, n = 67 neurons. (i, bottom) Location-selective only neurons (Loc.), n = 44, median = 1.84, range = 0.11 – 36.11 Hz. Odour and location selective neurons (Both): n = 23, median = 3.20, range = 0.26 – 20.23 Hz. (m) Population sparseness = 0.11 ± 0.05 ; lifetime sparseness = 0.16 ± 0.01 , Mean \pm S.D. (n = 15 sessions). (n) Population sparseness = 0.13 ± 0.08 ; lifetime sparseness = 0.20 ± 0.10 .

Article



Extended Data Fig. 5 | Population correlations matrices and single cell decoding accuracies. (a) Full similarity matrix of correlation coefficients of all odour and location population vector pairs for all recorded pPCx ($n=995$) and CA1 ($n=154$) neurons. Off-diagonal correlation coefficients on the lower right quadrants of each matrix show that CA1 location representations are more dissimilar from each other than pPCx location representations. Off-diagonal correlation coefficients on the top right and lower left quadrants show that there were no systematic relationship population responses for individual odours and locations. (b) Population correlation coefficients for odour and locations were shown in similarity matrices. Odour: top left quadrant; location: bottom right quadrant, excluding autocorrelation coefficients (diagonal band). Wilcoxon rank-sum test, ** $p < 0.01$, *** $p < 0.001$. (c) L1 regularization pseudo-population decoding curves in Fig. 2g (black lines) were overlaid on the same x-axis for comparison. (d) Cumulative distribution function of single cell decoding accuracies for all recorded pPCx (left) and CA1 (right) neurons show that individual pPCx neurons location is significantly better coding than odour. Kolmogorov-Smirnov test, *** $p < 0.001$.

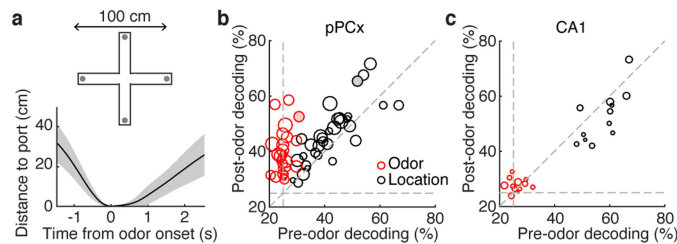


Extended Data Fig. 6 | Pseudo-population decoding. (a) Odour decoding accuracy for a simultaneously recorded pPCx population (example session from Fig. 2a–d) using a wide range of time windows aligned to odour onset time (left), or first respiration after odour onset (right). The black and red dots indicate time windows used for black and red lines in (c), respectively.

(b) Location decoding accuracy aligned to initiation port poke-in time across a wide range of time windows. (c) Pseudo-population decoding of odour identity with different time windows and regularization. Red and purple lines use L2 regularization, while black and grey use L1 regularization (shown as black and grey lines in Fig. 2g). By increasing the sparsity of the L1-decoder (scanning the ‘cost’ parameter over the range $2^{[-7:8]}$) and plotting decoding accuracy as a function of the number of contributing neurons (# of neurons with non-zero weights in the decoder), we can minimize the contribution of uninformative neurons. Here, the x-axis indicates the number of neurons being used by the decoder (i.e. neurons with non-zero kernel weights), which was controlled by

changing the L1 penalty. When this penalty is large, the decoder selectively uses only the most informative neurons, leading to a much steeper rise than seen for the L2 regularization pseudo-population curves, which sample neurons randomly. Using this sparse L1-decoding approach, it is clear that odour identity can accurately be decoded from a small population of pPCx neurons (90% decoding accuracy for ~150 neurons). Dotted line indicates 90% accuracy. Chance level is 25%. (d) Same analysis as in (c) but for port locations. Note that while it conveys that relatively few neurons are needed to encode odour information, the steepness of the grey curve is sensitive to the number of recorded neurons (since a larger pool is more likely to contain an informative neuron). (e, f) Yellow lines show pseudo-population decoding using neurons identified by auROC (see Methods) as responsive to either odour or location. Black and grey lines are the same as those plotted in (c, d), and Fig. 2g, reproduced here for ease of comparison.

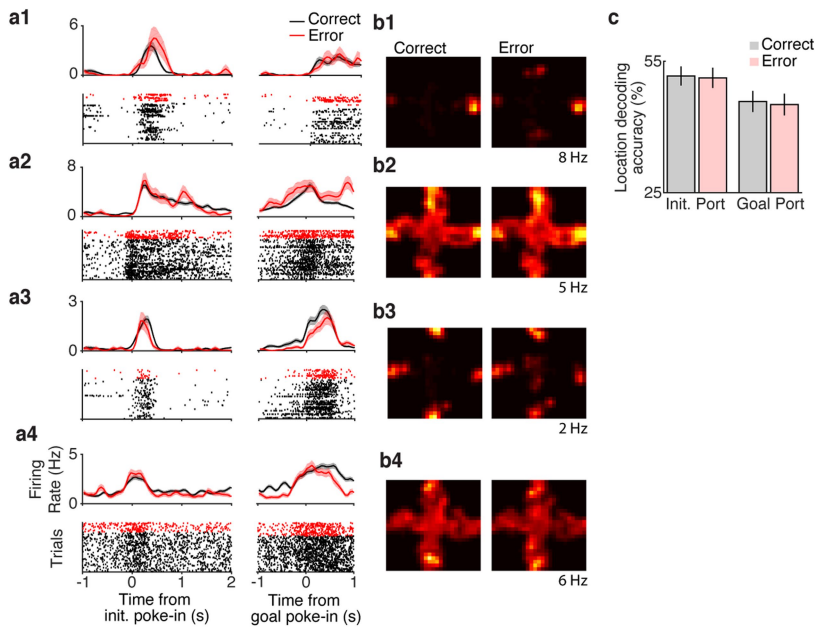
Article



Extended Data Fig. 7 | Location decoding accuracy is independent of olfactory drive.

(a) Distance from port locations aligned to odour onset.

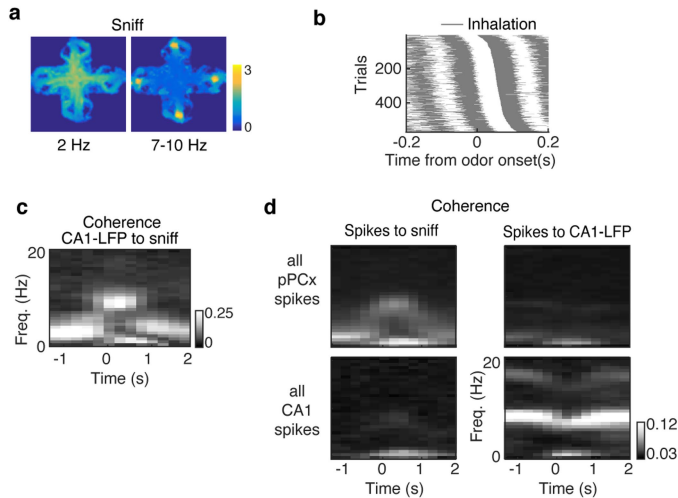
(b) Population decoding accuracy for odour and port locations across time for simultaneously recorded pPCx ($n = 33$ sessions; 8–53 cells/session). Pre-odour decoding used population activity from 1.5 s before odour onset; post-odour decoding used population activity 1.5 s after odour onset. Cross-validated, chance is 25%. The filled-in data points indicate the example session shown in Fig. 2. (c) Same analysis as in (b) for simultaneously recorded CA1 population ($n = 12$ sessions, 3–14 neurons/session).



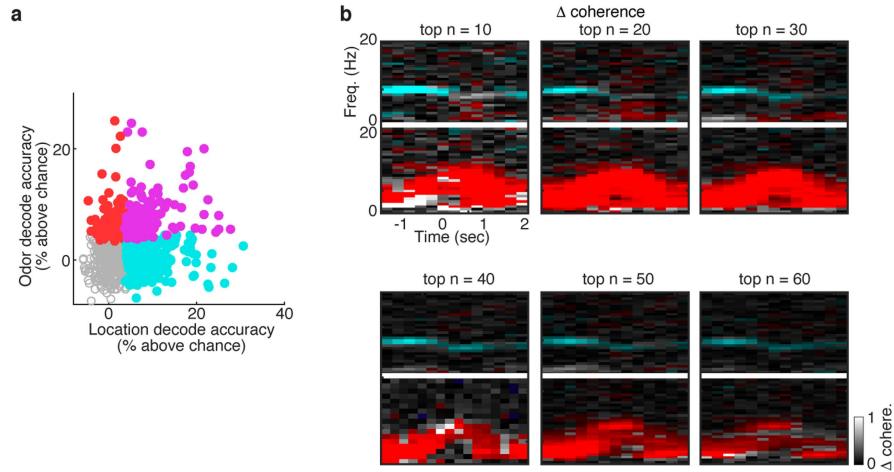
Extended Data Fig. 8 | Example cells and location decoding for correct and error trials. (a) PETH and rasters for 4 example neurons aligned to initiation port poke-in (left) and goal poke-in time (right). Black: correct trials; red: error trials. (b) Firing rate heat maps for example cells. Heat maps were normalized to occupancy and generated by concatenating all trials from -1 to 2 s window around initiation and goal port entry. Peak firing rates noted to the right of heat

maps. (c) Location decoding accuracy of a classifier trained on neural activity $-0.5 - 0.5$ s around initiation port poke-in for correct trials. The classifier was tested on neural activity $-0.5 - 0.5$ s around initiation and goal port poke-ins for correct (black) and error (red) trials (cross-validated, mean \pm S.E.M., $n = 33$ sessions; 30 ± 13 neurons/session).

Article



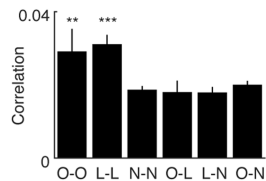
Extended Data Fig. 9 | Sniffing and hippocampal theta-band activity in task. (a) Sniffing behavior on maze in one example session. Heat map of basal sniffing behavior (2 Hz power) and high frequency active sniffing behavior (7-10 Hz power) on maze. Colorbar is power. (b) Sniffing behavior for one example session. Sniff phase was time-locked to odour port poke-in. Gray color is inhalation, white is exhalation. (c) Coherence between CA1-LFP and sniffing. Time is aligned to odour onset. Colorbar is coherence. (d, top) Average coherence of spike of all pPCx neurons to sniff (left) and CA1-LFP (right). Time is aligned to odour onset time. (d, bottom) Average coherence of spike of all recorded CA1 neurons to sniffing (left) and CA1-LFP (right).



Extended Data Fig. 10 | Preferential coupling of odour cells to sniffing and location cells to hippocampal theta. **(a)** Odour and location decoding accuracy of individual neurons. Neurons decoded odour only (red), location only (cyan), both (magenta), or neither (open circles). Decoding significance was defined as accuracy greater than the 95th percentile of classifiers trained on shuffled labels. **(b)** Mean difference in coherence between the ‘top n’ best odour decoding neuron vs ‘top n’ best location decoding neuron. Top panels of

each ‘top n’ analysis show differences in spike-sniff coherence, while bottom panels show differences in spikes-to-CA1-LFP coherence. Red pixels indicate frequency-time bins in which spikes from odour decoding cells are significantly more coherent than spikes from location decoding neurons, while blue pixels indicate the bins in which location cells are more significantly coherent than odour cells. Gray scale is coherence. (see Full Methods).

Article



Extended Data Fig. 11 | Noise correlations between pPCx neurons are consistent with distinct functional subgroups. Noise correlations between 3 groups of neurons (6 group pairings): odour-selective (O), location-selective (L), non-selective (N) neurons. Overall noise correlation between groups increased with longer time windows. O-O and L-L correlations are higher than for N-N. Mean \pm S.E.M., ** $p < 0.01$, *** $p < 0.001$.

Reporting Summary

Nature Research wishes to improve the reproducibility of the work that we publish. This form provides structure for consistency and transparency in reporting. For further information on Nature Research policies, see our [Editorial Policies](#) and the [Editorial Policy Checklist](#).

Statistics

For all statistical analyses, confirm that the following items are present in the figure legend, table legend, main text, or Methods section.

n/a Confirmed

- The exact sample size (n) for each experimental group/condition, given as a discrete number and unit of measurement
- A statement on whether measurements were taken from distinct samples or whether the same sample was measured repeatedly
- The statistical test(s) used AND whether they are one- or two-sided
 - Only common tests should be described solely by name; describe more complex techniques in the Methods section.*
- A description of all covariates tested
- A description of any assumptions or corrections, such as tests of normality and adjustment for multiple comparisons
- A full description of the statistical parameters including central tendency (e.g. means) or other basic estimates (e.g. regression coefficient) AND variation (e.g. standard deviation) or associated estimates of uncertainty (e.g. confidence intervals)
- For null hypothesis testing, the test statistic (e.g. F , t , r) with confidence intervals, effect sizes, degrees of freedom and P value noted
 - Give P values as exact values whenever suitable.*
- For Bayesian analysis, information on the choice of priors and Markov chain Monte Carlo settings
- For hierarchical and complex designs, identification of the appropriate level for tests and full reporting of outcomes
- Estimates of effect sizes (e.g. Cohen's d , Pearson's r), indicating how they were calculated

Our web collection on [statistics for biologists](#) contains articles on many of the points above.

Software and code

Policy information about [availability of computer code](#)

Data collection

We used the software package Bonsai2.3 for all video data collection. We used custom Matlab (2014b) code and real time Linux state machine (BControl) for collecting data from the peripheral devices contained in the behavioral apparatus. We used Blackrock cerebus recording system and software for collecting electrophysiology and sniffing data.

Data analysis

We used Bonsai2.3 for analysis of video data, and custom Matlab (2014b) and Python3.x code for the analysis of all other data.

For manuscripts utilizing custom algorithms or software that are central to the research but not yet described in published literature, software must be made available to editors and reviewers. We strongly encourage code deposition in a community repository (e.g. GitHub). See the Nature Research [guidelines for submitting code & software](#) for further information.

Data

Policy information about [availability of data](#)

All manuscripts must include a [data availability statement](#). This statement should provide the following information, where applicable:

- Accession codes, unique identifiers, or web links for publicly available datasets
- A list of figures that have associated raw data
- A description of any restrictions on data availability

The data and analysis code that support the findings of this study are available from the corresponding author upon reasonable request.

Field-specific reporting

Please select the one below that is the best fit for your research. If you are not sure, read the appropriate sections before making your selection.

- Life sciences Behavioural & social sciences Ecological, evolutionary & environmental sciences

For a reference copy of the document with all sections, see nature.com/documents/nr-reporting-summary-flat.pdf

Life sciences study design

All studies must disclose on these points even when the disclosure is negative.

Sample size	Sample sizes were not predetermined. Individual animals were highly trained over months. For behavioral analysis, the significance of effect for behavior was assessed for each animal. For electrophysiology, animals were included only if all tetrodes were located in the target regions by post-hoc histological analysis.
Data exclusions	All animals with performance over 75% were included in experiments, this value was predetermined. Single units (neurons) spike clustering quality were assessed manually. Units were only included if firing rate did not drift over the recording session, and spikes did not violate absolute refractory period.
Replication	All relevant behavioral effects were present in the majority of animals trained. Effects reported in neural data were consistent across animals, and significant at the appropriate group level within the nested structure of the data.
Randomization	Within our olfactory spatial choice task, reward contingency for individual odors were fixed across animals (e.g. odor 1 indicates North reward port). However, the sequence of trajectories (determined by initiation port location and odor identity) were randomized in each session and across animals. This randomized trajectory of trials guaranteed that no bias was created from training protocol.
Blinding	We did not have separate behavioral group allocations. Given the fact that this study involved a difficult behavioral task, with targeted large population of electrophysiological recordings in a challenging brain region, to guarantee that we had sufficient numbers of animals and neurons, researchers needed to know the behavioral performance and recording location outcome.

Reporting for specific materials, systems and methods

We require information from authors about some types of materials, experimental systems and methods used in many studies. Here, indicate whether each material, system or method listed is relevant to your study. If you are not sure if a list item applies to your research, read the appropriate section before selecting a response.

Materials & experimental systems	Methods
n/a	Involved in the study
<input checked="" type="checkbox"/>	<input type="checkbox"/> Antibodies
<input checked="" type="checkbox"/>	<input type="checkbox"/> Eukaryotic cell lines
<input checked="" type="checkbox"/>	<input type="checkbox"/> Palaeontology and archaeology
<input type="checkbox"/>	<input checked="" type="checkbox"/> Animals and other organisms
<input checked="" type="checkbox"/>	<input type="checkbox"/> Human research participants
<input checked="" type="checkbox"/>	<input type="checkbox"/> Clinical data
<input checked="" type="checkbox"/>	<input type="checkbox"/> Dual use research of concern
n/a	Involved in the study
	<input checked="" type="checkbox"/> ChIP-seq
	<input checked="" type="checkbox"/> Flow cytometry
	<input type="checkbox"/> MRI-based neuroimaging

Animals and other organisms

Policy information about [studies involving animals: ARRIVE guidelines](#) recommended for reporting animal research

Laboratory animals	Rattus norvegicus domestica, male Long Evans rats, aged between 3-9 months (>250g in weight) were used.
Wild animals	n/a
Field-collected samples	n/a
Ethics oversight	The study protocol was approved by the Champalimaud Foundation Animal Welfare Committee, the Portuguese national veterinary agency, and in accordance with current European Union law.

Note that full information on the approval of the study protocol must also be provided in the manuscript.